Transition from bainite to acicular ferrite in reheated Fe–Cr–C weld deposits

Factors controlling the transition from acicular ferrite to bainite in Fe–Cr–C weld metals have been investigated. It appears that the presence of allotriomorphs of ferrite at austenite grain boundaries has the effect of suppressing the formation of bainitic sheaves. This in turn allows the acicular ferrite plates to develop on intragranular nucleation sites. A theoretical analysis indicates that bainitic transformation is prevented from developing at the allotriomorphic ferrite/austenite boundaries by the carbon concentration field present in the austenite at the allotriomorphic ferrite/austenite interface. This field does not homogenise within the residual austenite during the time scale of the experiments. *MST/1217*

S. S. Babu
H. K. D. H. Bhadeshia

© *1990 The Institute of Metals. Manuscript received 5 March 1990.* *The authors are in the Department of Materials Science and Metallurgy, University of Cambridge.*

Introduction

The results presented here are part of a programme of research aimed at the prediction of the microstructure and properties of low alloy steel weld deposits. In many steel weld deposits, a reduction of allotriomorphic ferrite and Widmanstätten ferrite leads to a corresponding increase in the amount of acicular ferrite. This behaviour has been demonstrated to be consistent with phase transformation theory. However, it has been suggested that there is an anomaly in the development of microstructure in Fe–Cr–Mo–C weld deposits.[1] For example, Evans[2,3] reported that, as the chromium or molybdenum concentration was increased, the amount of allotriomorphic ferrite decreased, but, at the same time, the volume fraction of acicular ferrite was found to go through a maximum as a function of the chromium or molybdenum content. This effect is shown in Fig. 1. Therefore, the volume fraction of the remainder of the microstructure, which Evans described as 'ferrite with aligned second phase', increases with concentration. The term 'ferrite with aligned second phase' describes a microstructure consisting of regions in which plates of ferrite have approximately parallel habit planes (i.e. are aligned), the individual plates being separated by residual phases such as retained austenite, martensite, or carbides. It actually refers to bainite and/or Widmanstätten ferrite. Since the latter phase is known to decrease with chromium and molybdenum additions,[4] it has been suggested recently[1] that the actual reason why the volume fraction of acicular ferrite goes through a maximum is that it is replaced progressively by bainite, with the combined fraction of acicular ferrite and bainite actually increasing with solute concentration. The proposed effect is shown in Fig. 1 which is a modified representation of Evans' data, in which the field that he designated originally as ferrite with aligned second phase is subdivided schematically into regions A and B, the latter representing bainite and the former Widmanstätten ferrite. Thus, the reduction in acicular ferrite content at high concentrations of chromium and molybdenum is suggested to be a result of a corresponding increase in the bainite content as the volume fraction of allotriomorphic ferrite and Widmanstätten ferrite decreases.

This hypothesis is consistent with the well established fact that Fe–2·25Cr–1Mo–C (wt-%) weld deposits of the type used in power plant have an almost completely bainitic microstructure in the as deposited condition.[5–7] As will be seen below, it is possible in hindsight to find many examples of this phenomenon (i.e. replacement of acicular ferrite by bainite as the solute concentration is increased) in the published literature on steel weld deposits. To investigate the mechanism behind this transition and to find possible ways of enhancing the acicular ferrite content in such Fe–Cr–Mo–C weld metals, controlled phase transformation studies have been carried out in the present work using Fe–C–Cr weld metals. The primary aim was to elucidate the mechanism of the transition from acicular ferrite to bainite in these weld deposits, so that the microstructure model[8] could be modified to predict such effects.

Recent work on acicular ferrite[8–10] indicates that acicular ferrite appears to be *intragranularly nucleated bainite*, in which the development of aggregates of parallel plates (the classical sheaves of bainite) is suppressed by the hard impingement of acicular ferrite plates nucleating from adjacent sites. Thus, bainite sheaves develop when they

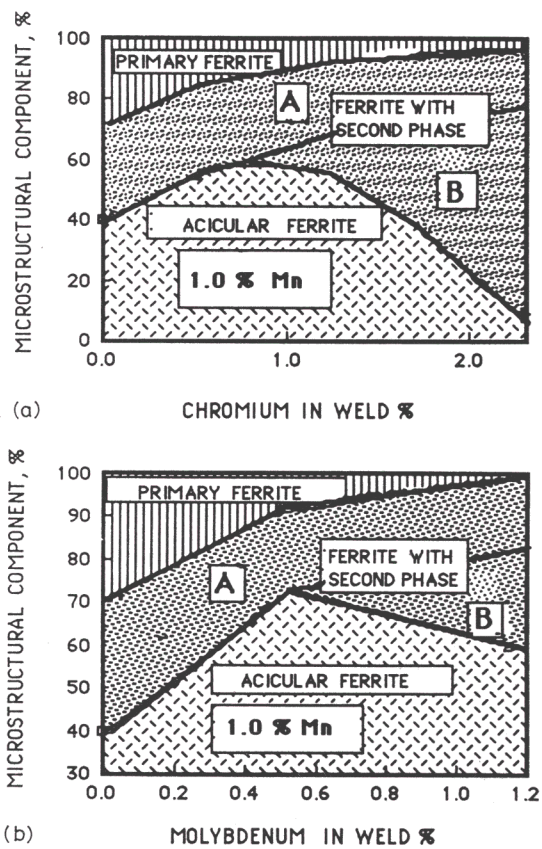

1 Effect of *a* chromium and *b* molybdenum on C–Mn primary weld metal microstructure (data from Refs. 2, 3); 'ferrite with second phase' region is here divided schematically into two regions to separate Widmanstätten ferrite (A) from bainite (B)[1]

can nucleate at the austenite grain surfaces, whereas the intragranularly nucleated bainite is, in effect, acicular ferrite. Thus, a reduction in inclusion density leads to a transition from acicular ferrite to bainite as demonstrated by Harrison and Farrar.[11] Alternatively, an increase in the density of austenite grain boundary nucleation sites leads to the same transition.[9] These studies emphasise the dependence of the transition on the relative amounts of austenite grain boundary and intragranular nucleation sites available when the weld metal reaches a transformation temperature below the bainite start temperature B_s.

Based on this current knowledge of the factors favouring bainite versus acicular ferrite, it was considered that bainitic microstructure begins to dominate at high solute concentration, perhaps because the usual allotriomorphic ferrite layers then begin to diminish, leaving the austenite grain surfaces exposed for the nucleation of bainite. Therefore, the work reported here had the intention of identifying any role of allotriomorphic ferrite in the transition from a predominantly bainitic microstructure to a microstructure containing a large amount of acicular ferrite. Allotriomorphic ferrite grows as layers on the prior austenite grain boundaries and, since it is the first phase to grow on cooling from the austenite phase field, it should cause a reduction in the number density of austenite grain boundary nucleation sites and, hence, promote the preferential formation of acicular ferrite at the expense of bainite. At first this appears to be consistent with the behaviour of the Fe–Cr–Mo–C welds, if it is assumed that the chromium and molybdenum prevent the formation of allotriomorphic ferrite at high concentrations and, hence, lead to the promotion of classical bainite at the expense of acicular ferrite.

Experimental techniques

ALLOYS

The samples were machined from the weld metal portion of an all weld metal testpiece. The weld itself was fabricated according to the international standard ISO 2560, ensuring that the weld geometry is compatible with the minimisation of dilution effects associated with the melting of the base plate. The weld metal was deposited using the manual metal arc welding technique. The welding parameters used and the weld composition are given in Tables 1 and 2, respectively. The samples machined from the weld were hot rolled and swaged to rods of 3 mm diameter and 15 mm length. Some of these cylindrical samples were drilled subsequently along the cylinder axes to give 1·5 mm diameter bores to accelerate the cooling rate that could be achieved during dilatometric experiments. To minimise any effects of chemical segregation, the specimens were then homogenised by annealing at 1200°C for 3 days, while protected by being sealed in quartz tubes, each containing a partial pressure of pure argon. After annealing, the samples were quenched in an ice-water mixture.

FURNACE HEAT TREATMENTS

The main aim of the present investigation was to study the influence of prior allotriomorphic ferrite formation on the austenite/austenite grain boundaries, on subsequent transformation below B_s. To plan the heat treatments, a phase diagram and a time–temperature–transformation (TTT) diagram were calculated for the alloy given in Table 2, the calculation taking into account the carbon, silicon, manganese, nickel, molybdenum, and chromium concentrations, using a method published elsewhere.[12,13] The bainitic ferrite B_s, Widmanstätten ferrite W_s, and martensitic M_s start temperatures were also calculated using the same method (Fig. 2). The equilibrium transformation temperature Ae_3 was calculated as in Sugden and Bhadeshia.[14] The transformation temperature data are given in Table 3.

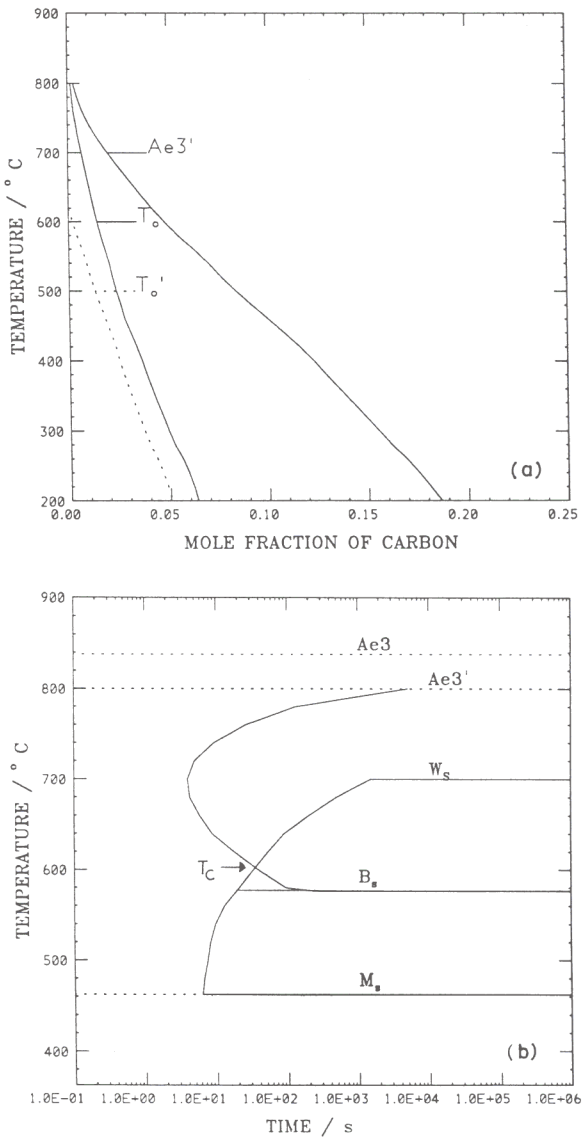

Ae_3, Ae_3' upper limiting temperature of $\alpha + \gamma$ phase field at equilibrium, paraequilibrium; T_0 temperature at which ferrite and austenite of identical composition have same free energy; T_0' as T_0, but taking into account strain energy of ferrite

2 Calculated *a* phase diagram and *b* TTT diagram based on model developed by Bhadeshia[12,13] for Fe–0·053C–0·51Si–1·11Mn–1·59Cr (wt-%) weld metal

Table 1 Welding process parameters

Welding voltage, V	23
Welding current, A	120
Welding speed, m s^{-1}	0.004
Interpass temperature, °C	250

Table 2 Weld metal composition, wt-%

Alloy	C	Si	Mn	Cr	Mo	Ni	N*	O*
78	0·053	0·51	1·11	1·59	0·01	0·03	118	366

*Values are given in ppm.

Table 3 Calculated transformation data for alloy 78

Ae_3, °C	838
W_s, °C	700
B_s, °C	578
M_s, °C	464

The experiments involved the isothermal reaction of austenite at two successive temperatures T_1 and T_2. The heat treatment at T_1 was intended to allow the formation of some allotriomorphic ferrite, so that the austenite grain boundaries would be covered by a thin layer of the ferrite. The remainder of the austenite could then be transformed at a temperature T_2 below B_s. For purposes of comparison, the heat treatment at T_1 was omitted for some samples, the austenite being quenched directly to T_2 to avoid the formation of any allotriomorphic ferrite.

Based on the data from the calculated TTT diagram, heat treatments F1 and F2 were planned as described in Table 4; the prefix F refers to experiments carried out using a resistance heated furnace. Three furnaces were maintained at the required temperatures: one for austenitising at a temperature T_γ and the other two for isothermal heat treatments at T_1 and T_2. During the heat treatments, the samples were transferred rapidly between furnaces. Preliminary studies revealed that, owing to relatively low cooling rates associated with such transfers, allotriomorphic ferrite formation could not be avoided in specimen F1 while cooling from T_γ to T_2. In addition, heat treatment at $T_1 = 700$°C was found to lead to the rapid growth of allotriomorphic ferrite to a very large volume fraction ($\sim 0{\cdot}75$) after only 5 min at T_1. This defeats the purpose of the experiment which was to decorate the austenite grain surfaces with *thin* layers of ferrite which would not consume the bulk of the austenite, leaving it free to decompose into intragranularly nucleated acicular ferrite.

To overcome these difficulties, the driving force for allotriomorphic ferrite growth was reduced by raising T_1, and the cooling rate from T_1 to T_2 was increased by increasing further the difference $T_1 - T_2$ by reducing T_2 to 470°C. These changes are not sufficient in themselves to prevent the formation of allotriomorphic ferrite in the interval between T_1 and T_2, but that is not important, providing a thin covering of allotriomorphic layer is observed at the austenite grain surfaces before T_2 is attained. The calculated data on the transformation behaviour expected for the present alloy (*see* Table 5) also suggest the scale of incubation time available at that particular temperature. The modified experiments (F3–F8) gave some results of interest which will be discussed below. The heat treatment schedules are shown schematically in Fig. 3.

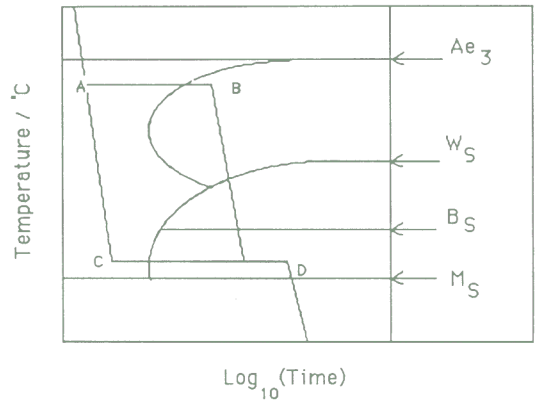

3 Schematic diagram of furnace heat treatments: paths ABD and ACD show two step and single step heat treatments, respectively; three resistance heated furnaces were used

DILATOMETRY

The advantage of dilatometry is that it enables transformations to be recorded as they occur. The volume change associated with a phase transformation can be followed by monitoring the change in length, which, over the temperature region of interest, can provide information about the transformation temperatures and the reaction kinetics. The length change during transformation was recorded using a Theta Industries high speed dilatometer, equipped with a water cooled induction furnace which has an essentially zero thermal mass. The dilatometer has been interfaced with a BBC/Acorn computer, which is used for programming the thermal cycles and also for collecting and recording length change, time, and temperature data automatically. For the dilatometric studies, the homogenised specimens were electroplated with a 0·08–0·1 mm thick layer of nickel to avoid surface degradation and surface nucleation effects.[16]

The volume fraction of transformation is related to the length change detected by the dilatometer. For bainitic transformation involving no precipitation of carbides, the relation is given by the following equation[17]

$$\frac{\Delta L}{L} \simeq \frac{[2Va_\alpha^3 + (1-V)a_\gamma^3 - \bar{a}_\gamma^3]}{3\bar{a}_\gamma^3} \quad \ldots\ldots\ldots \quad (1)$$

where $\Delta L/L$ is the relative length change due to transformation; V is the volume fraction of ferrite; a_α is the lattice parameter of ferrite (a function of temperature) given by

$$a_\alpha = \bar{a}_\alpha[1 + e_\alpha(T - 298)] \quad \ldots\ldots\ldots \quad (2)$$

where T is the absolute temperature, $\bar{a}_\alpha$ is the lattice parameter of ferrite at ambient temperature (25°C), and e_α is the linear thermal expansion coefficient of ferrite; $\bar{a}_\gamma$ is the calculated lattice parameter of austenite at the mean alloy composition (i.e. when $V = 0$) given by

$$\bar{a}_\gamma = \left(a_\gamma^\circ + \sum_{i=1}^{n} C_i x_i\right)[1 + e_\gamma(T - 298)] \quad \ldots\ldots \quad (3)$$

where a_γ° is the lattice parameter of unalloyed austenite, e_γ is the linear thermal expansion coefficient of austenite, and

Table 4 Details of furnace heat treatments

Treatment	T_γ, °C	Time at T_γ, min	T_1, °C	Time at T_1, min	T_2, °C	Time at T_2, min	Quench condition
F1	1150	20	...	...	500	2	Ice–water
F2	1150	20	700	5	500	2	Ice–water
F3	1150	30	...	...	470	2	Ice–water
F4	1150	30	800	10	470	2	Ice–water
F5	1150	30	800	5	470	2	Ice–water
F6	1150	30	...	...	...	...	Continuous cooling*
F7	1150	30	800	10	600	2	Ice–water
F8	1150	30	800	10	...	...	Ice–water

*The cooling rate could not be measured, since the samples were sealed in quartz tubes, but was estimated to be about 50 K s^{-1}.

Table 5 Phase diagram and TTT diagram details at selected temperatures

Temperature, °C	$x^{\gamma\alpha}$	$x^{\alpha\gamma}$	$\underline{D}$, cm^2 s^{-1}	α_1, cm s$^{-1/2}$	τ, s
800	0·0029	0·00042	$0{\cdot}177 \times 10^{-7}$	$0{\cdot}262 \times 10^{-4}$	$0{\cdot}51 \times 10^{4}$
760	0·0073	0·000542	$0{\cdot}7628 \times 10^{-8}$	$1{\cdot}526 \times 10^{-4}$	$0{\cdot}26 \times 10^{2}$
720	0·0150	0·000633	$0{\cdot}4416 \times 10^{-8}$	$2{\cdot}204 \times 10^{-4}$	$0{\cdot}5 \times 10^{1}$
680	0·0251	0·000698	$0{\cdot}2375 \times 10^{-8}$	$2{\cdot}321 \times 10^{-4}$	$0{\cdot}43 \times 10^{1}$
640	0·0362	0·000738	$0{\cdot}1291 \times 10^{-8}$	$2{\cdot}157 \times 10^{-4}$	$0{\cdot}88 \times 10^{1}$
600	0·0483	0·000754	$0{\cdot}0668 \times 10^{-8}$	$1{\cdot}838 \times 10^{-4}$	$0{\cdot}39 \times 10^{2}$

$x^{\gamma\alpha}$ is the carbon concentration in austenite which is in paraequilibrium with ferrite at the temperature concerned, in units of mole fraction.
$x^{\alpha\gamma}$ is the carbon concentration in ferrite which is in paraequilibrium with austenite at the temperature concerned, in units of mole fraction.
α_1 is the one dimensional parabolic thickening rate constant for paraequilibrium growth of allotriomorphic ferrite.
τ is the incubation time required for a detectable amount of transformation to ferrite from austenite.
$\underline{D}$ is the weighted average diffusivity calculated by considering the carbon concentration profile in front of the moving ferrite interface, as given by the following equation:[15] $\underline{D} = \int_{x^{\alpha\gamma}}^{\bar{x}} D\{X\}/(\bar{x} - x^{\gamma\alpha})$, where $\bar{x}$ is the average composition of the alloy and X is the distance ahead of the moving ferrite interface.

C_i are coefficients relating alloying element concentration x_i to the lattice parameter, where $i = 1, 2, \ldots, n$ denotes various alloying elements ($i = 1$ for carbon); and a_γ is the calculated lattice parameter of austenite taking account of the carbon enrichment in austenite when $V \neq 0$ given by

$$a_\gamma = \left[a_\circ + C_1 \frac{(\bar{x} - Vx^{\alpha\gamma})}{(1-V)} + \sum_{i=1}^{n} C_i x_i \right] [1 + e_\gamma (T - 298)] \quad \ldots\ldots\ldots\ldots \quad (4)$$

where $x^{\alpha\gamma}$ is assumed to be given by the equilibrium concentration of carbon in ferrite in Fe–C alloys, as estimated using a quasichemical thermodynamic model[18,19] (Table 5), and $\bar{x}$ is the mean carbon concentration of the alloy in mole fraction.

The dilatometric experiments were directed towards the investigation of the 'incomplete reaction' phenomenon of the type reported for acicular ferrite and bainite in weld alloys by Yang and Bhadeshia[9] and Strangwood and Bhadeshia.[10] This would help to verify that the transformation products which form at T_2 correspond to the reported thermodynamic characterisation of bainite or acicular ferrite. Samples were austenitised at two different temperatures (1000°C for 10 min or 1150°C for 10 min) to obtain a small or large austenite grain size to induce a predominantly bainite or acicular ferrite microstructure, respectively, when subsequently transformed isothermally below the calculated B_s temperature. Thus, the experiment was designed to change the relative number densities of austenite grain boundary versus intragranular nucleation sites. Some details of the dilatometric experiments are given in Table 6.

MEASUREMENT OF LINEAR THERMAL EXPANSION COEFFICIENTS

It is evident that a knowledge of the coefficients e_α and e_γ is necessary for computing the volume fraction of transformation as a function of the dilatometric length change. To measure the expansion coefficient of ferrite, dilatometer specimens were first tempered for 1 h at 600°C to ensure an essentially ferritic microstructure. The length change data recorded during slow heating to 600°C and cooling from 600°C (~ 4 K s^{-1}) were then analysed to estimate the linear expansivity.

For austenite, length change data recorded during heating from 850 to 1000°C, at a rate of 10 K s^{-1}, in the austenite phase field were analysed. The expansion coefficients measured in this way (*see* Fig. 4) were found to be: $e_\alpha = 1{\cdot}4026 \times 10^{-5} \pm 0{\cdot}35 \times 10^{-7}$ K^{-1} and $e_\gamma = 1{\cdot}8854 \times 10^{-5} \pm 0{\cdot}12 \times 10^{-7}$ K^{-1}. These values were constant over the temperature ranges studied, as indicated by correlation coefficients greater than 0·99 obtained when the length change versus temperature data were subjected to linear regression analysis.

LATTICE PARAMETERS

The lattice parameter values necessary for the interpretation of dilatometric data were measured for ferrite for a sample tempered at 600°C for 1 h, using the Debye–Scherrer X-ray diffraction method with Cu $K\alpha$ radiation, the accelerating voltage being 45 kV and the tube current 25 mA. Since the Cu $K\alpha_1$ and Cu $K\alpha_2$ lines could not be resolved, an average wavelength 1·5424 Å was used for the analysis. A specimen of 0·5 mm diameter was prepared by machining carefully from a 3 mm diameter rod, and its surface layer was removed by soaking in a chemical polishing mixture of 5%HF:50%H_2O_2:45%H_2O for 10 min; this procedure leads to more accurate parameter measurements, since the effects of deformation induced by machining are removed. The Bragg angles θ were measured from the 011, 002, 112, 022, and 013 reflections and the data were plotted against the Nelson–Riley extrapolation function using a least squares linear regression procedure. Since errors decrease with increasing θ, the data were weighted using a $1/\cos^2\theta$ function during regression analysis.[20] The extrapolation procedure is shown in Fig. 5. The ferrite lattice parameter was found to be $2{\cdot}8679 \pm 0{\cdot}106 \times 10^{-2}$ Å. Using the relations given by Leslie[21] and Wever[22] and using a program which again takes into consideration the equilibrium dissolved carbon in ferrite,[23] the lattice parameter

Table 6 Experimental details of dilatometric tests

Experiment	T_γ, °C	Time at T_γ, s	T_i, °C	Time at T_i, min	T_s, °C	Δt_{850-T_i}, s	Cooling condition
S1	1000	600	505	60	774	4·5	Quench
S2	1000	600	519	60	785	5·3	Quench
L1	1150	600	513	60	660	7·6	Quench
L2	1150	600	529	60	665	14·8	Quench

L, S denote the transformation from large and small austenite grain sizes, respectively. The grain sizes measured for low T_γ and high T_γ samples were 41 ± 5 μm ($T_\gamma = 1000$°C) and 71 ± 6 μm ($T_\gamma = 1150$°C), respectively, as measured using the thermal grooving method.
T_i is the isothermal heat treatment temperature.
T_s is the temperature at which allotriomorphic ferrite formation begins during cooling of austenite.
Δt_{850-T_i} is the time required to cool sample from 850°C to T_i.

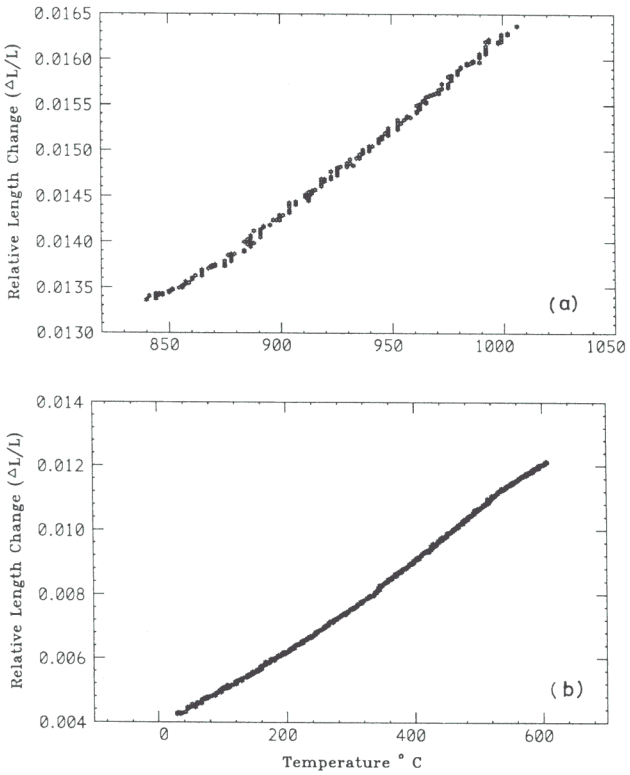

4 Typical data used for measurement of *a* austenite and *b* ferrite linear thermal expansion coefficients; correlation coefficients of data were found to be greater than 0·99, when subjected to linear regression analysis

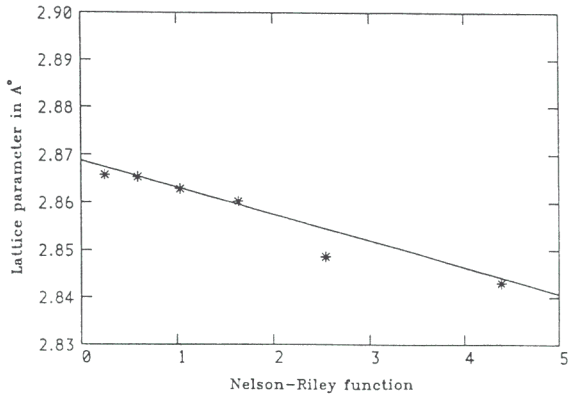

5 Lattice parameter measurement by extrapolation of Nelson-Riley function (*see* text): points represent lattice parameter measured from angles measured from various sets of planes; solid line is fitted line with weighting; and intercept at *y* axis for Nelson–Riley function of zero gives lattice parameter of ferrite

of ferrite was calculated and found to be 2·8679 Å, which is in excellent agreement with the experimental value. The equation for predicting the ferrite lattice parameter is

$$\bar{a}_\alpha = a^\circ_{Fe} + e_C - (3{\cdot}0 \times 10^{-12})M_{Si} + (6{\cdot}0 \times 10^{-12})M_{Mn} + (7{\cdot}0 \times 10^{-12})M_{Ni} + (0{\cdot}31 \times 10^{-10})M_{Mo} + (5{\cdot}0 \times 10^{-12})M_{Cr} + (0{\cdot}096 \times 10^{-10})M_V \quad . \; . \; (5)$$

where M_{Si}, M_{Mn}, etc. are mole fractions of alloying elements, a°_{Fe} is the lattice parameter of pure iron, taken to be 2·8664 Å, and e_C is the expansion in lattice parameter due to carbon dissolved in the ferrite.

TRANSMISSION ELECTRON MICROSCOPY (TEM)

Thin foils of selected heat treated specimens were prepared for TEM. After slicing into thin discs of 0·3 mm thickness, the discs were thinned to 60–80 μm by abrasion using SiC coated grinding paper and electropolished using an electrolyte consisting of a mixture of 5% perchloric acid: 25% glycerol: 70% ethyl alcohol. The polishing potential was 65 V at a current of 18–25 mA and the electrolyte temperature range was 0–10°C. The thin foils were examined using a Philips EM-300 or EM-400T TEM operated at 100 and 120 kV, respectively.

Thin film extraction carbon replicas were also prepared from the samples. Replicas were prepared by vapour deposition of carbon onto the sample in a vacuum chamber. The carbon film was stripped from the surface of the sample by etching the matrix in 5% chloral (5% concentrated HCl in ethanol) solution. The replicas were mounted onto copper grids and were observed in the TEM.

Thin film foils or replicas were mounted onto a low background specimen holder and tilted at a 35° take-off angle in the microscope column during energy dispersive X-ray analysis (EDX). The X-ray energy spectra were analysed using a LINK-RTS2 analyser program. The program calculates the relative amount of elements present in a test by fitting observed energy spectra to a standard spectrum. The program is also capable of separating overlapping peaks and giving a thickness correction. The spot size used in analysis was about 2 nm. Owing to absorption effects in the specimen, the beam broadening was estimated to be about 20 nm.

SCANNING ELECTRON MICROSCOPY (SEM)–EDX

The transformed sample F5 was also imaged in a SEM operated at 25 kV and equipped with an EDX analyser. The specimen was tilted at a take-off angle of 45°. The accelerating voltage was reduced to 20 kV for EDX analysis. The energy spectra were analysed using the LINK-RTS2-FLS program capable of giving ZAF (Z = atomic number, A = absorption, F = fluorescence) corrections.

LIGHT MICROSCOPY AND MICROHARDNESS TESTING

Metallographic observations were made on samples polished mechanically and etched in 2% nital and volume fraction measurements were carried out using a Swift point counter at a magnification of 400×, with 1000 points for each specimen. The austenite grain sizes were measured either directly on the metallographic samples when the boundaries were made clearly visible by layers of allotriomorphic ferrite or using a thermal grooving method. In the latter method, metallographically polished specimens were austenitised in a protective helium atmosphere in the dilatometer chamber, and the thermal grooves, which develop as the grain boundaries and free surface tension terms balance, can be used to reveal the positions of the grain boundaries. The grain sizes were defined using the typical mean linear intercept method. Some of the transformed samples were hardness tested in a Leitz–Vickers microhardness tester with a force of 0·981 N.

Results

EFFECT OF ALLOTRIOMORPHIC FERRITE

The microstructures obtained in samples F3–F5 and corresponding TEMs of selected specimens are shown in

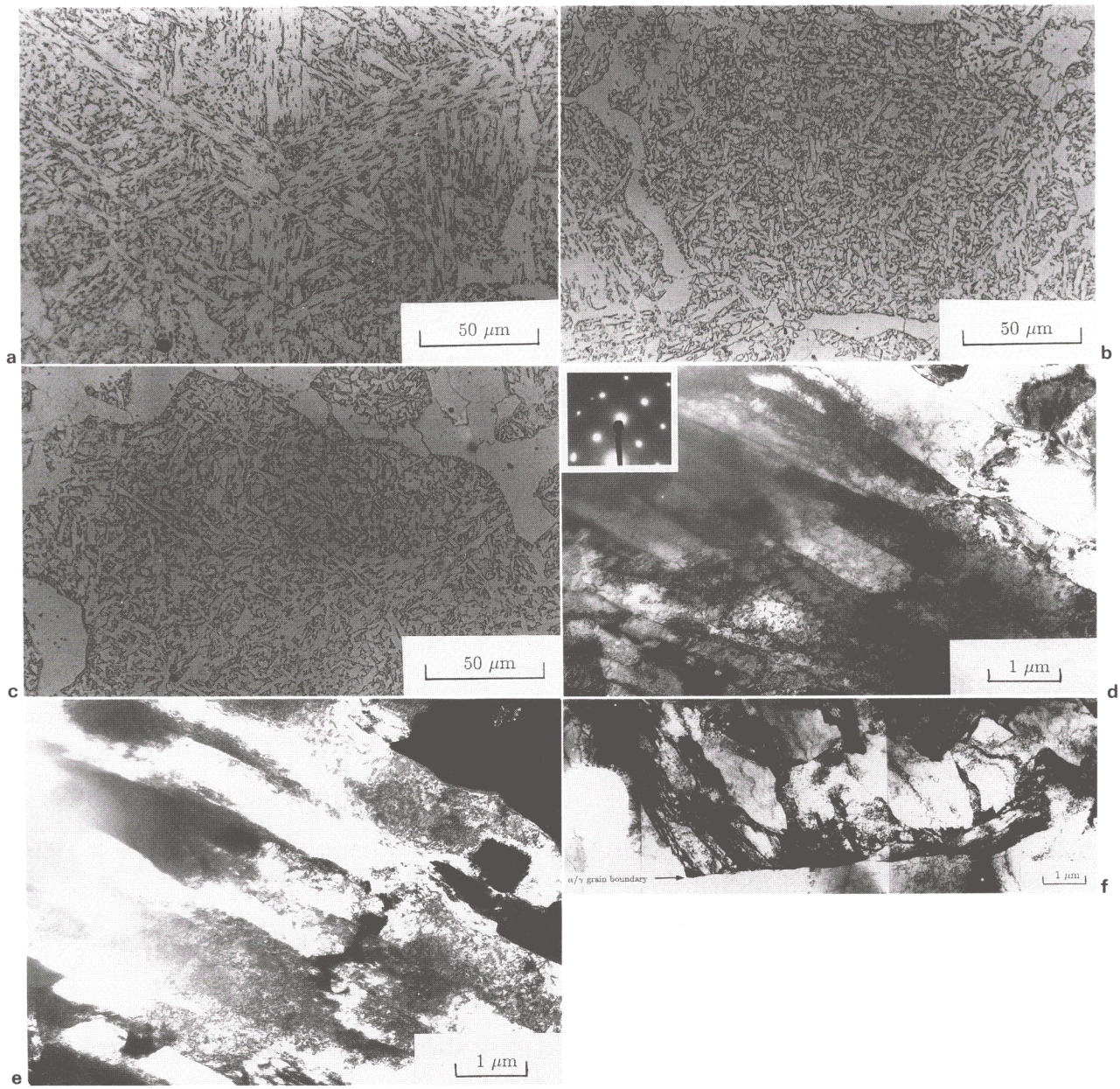

a F3: microstructure showing bainitic sheaf structure (microhardness was 278 HV); *b* F4: microstructure of acicular ferrite and grain boundary allotriomorphic ferrite (hardness of acicular ferrite region was 285 HV); *c* F5: microstructure of allotriomorphic ferrite and acicular ferrite – note that thickness of allotriomorphic ferrite is greater than in F4 (hardness measured in acicular ferrite region was 283 HV); *d* F3: bright field TEM showing sheaf structure of bainite (inset is diffraction pattern from ⟨001⟩ ferrite zone axis); *e* F3: corresponding dark field TEM using (020) spot showing that bainitic platelets within sheaf are all in same crystallographic orientation; *f* F5: microstructure showing possible acicular ferrite nucleation away from α/γ interface (dark phase could be martensite transformed from carbon enriched austenite)

6 Microstructures obtained in furnace experiments F3–F5

Fig. 6. The microstructures obtained in samples F6–F8 and a TEM of sample F6 are shown in Fig. 7.

The optical microstructure of specimen F3 revealed classic bainite sheaves, consisting of aggregates of small parallel plates, a result confirmed using TEM (Figs. 6*d* and 6*e*); this was the expected result, i.e. all platelets within a sheaf have identical crystallographic orientation.[24,25] This is consistent with the fact that the sample had been transformed directly to bainite without the intervening isothermal hold at T_1, which would have caused the formation of allotriomorphic ferrite; thus, the bainite sheaves nucleate at the undecorated austenite grain boundaries. In contrast, samples F4 and F5, which had been given a two stage heat treatment, showed very different final microstructure, consisting of layers of allotriomorphic ferrite and intragranularly nucleated acicular ferrite (Figs. 6*b*, 6*c*, 6*f*). It can be seen that the allotriomorphic ferrite destroys the original austenite grain boundary nucleation sites and thereby forces heterogeneous nucleation of acicular ferrite on intragranular inclusions.

To demonstrate that such drastic changes in microstructure cannot be explained by austenite grain size and variations in the present studies, the austenite grain sizes of specimens F5 and F6 were measured and found to be 70 ± 10 μm for F5 and 76 ± 11 μm for F6. As expected, the measurements are identical within the limits of experimental error. The apparent thickness of allotriomorphic ferrite of about 5–10 μm when compared with the austenite grain size shows that, for most specimens studied, there is sufficient austenite remaining for further transformation at T_2, a condition essential for the intragranular formation of acicular ferrite.

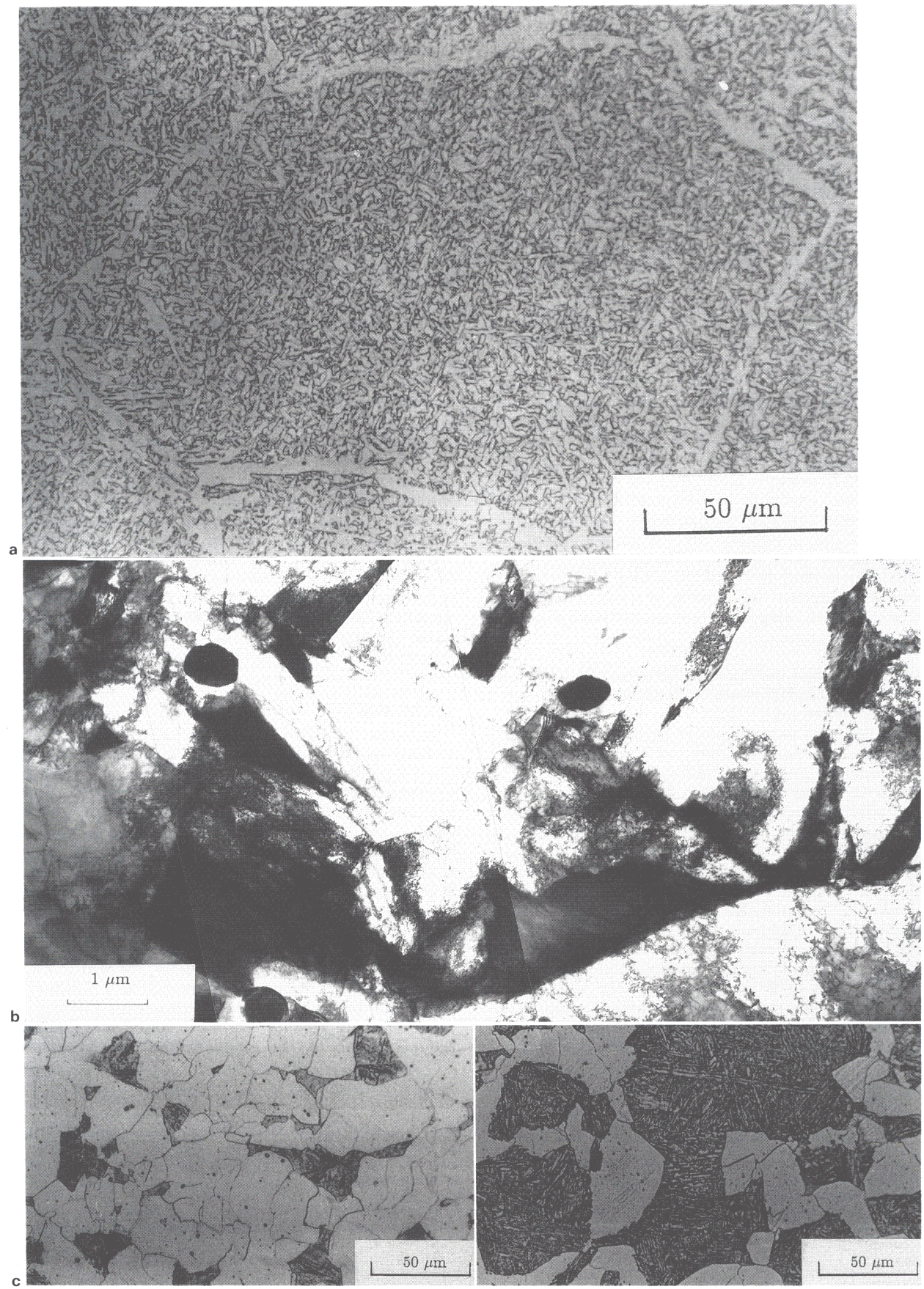

a F6: microstructure on transformation by continuous cooling (note similarity between this microstructure and typical weld microstructures that develop in ordinary C–Mn weld metals); *b* F6: typical microstructures developed close to α/γ interface showing allotriomorphic ferrite and acicular ferrite colony away from interface (dark phase could be martensite formed from carbon enriched austenite); *c* F7: microstructure developed by transformation above B_s ($T_2 = 600°C$ after $T_1 = 800°C$) which is essentially allotriomorphic ferrite and martensite; *d* F8: residual austenite islands transformed to martensite by quenching after $T_1 = 800°C$, proving that acicular ferrite morphology develops only by transformation below B_s (hardness measured in martensitic region was 352 HV and that of allotriomorphic ferrite was 193 HV)

7 Microstructures obtained in furnace experiments F6–F8

Further experiments were carried out to confirm that acicular ferrite does not form in this alloy unless the transformation temperature T_2 is less than B_s. Specimen F7 was first transformed partially to a similar amount of allotriomorphic ferrite at $T_1 = 800°C$ in the usual way and then quenched to a higher value of $T_2 = 600°C$, which is above B_s. The microstructure obtained (Fig. 7*c*) shows clearly that transformation above B_s leads simply to the formation of more allotriomorphic ferrite, while any small amount of untransformed austenite decomposes martensitically on cooling to ambient temperature. The microstructure consists essentially of equiaxed allotriomorphic ferrite and small islands of martensite which would have formed on quenching after the second isothermal heat treatment. The results were confirmed further by sample F8 (Fig. 7*d*), which was quenched without any second isothermal heat treatment; allotriomorphic ferrite is again observed as for F7 (or F4, F5), but its volume fraction is found to be less than in F7 owing to the absence of the isothermal reaction at 600°C. The residual austenite has again transformed into martensite instead of acicular ferrite. The result supports the concept that the acicular ferrite microstructure does not form by transformation above B_s.

The volume fractions of allotriomorphic ferrite in samples F4 and F5 were measured to be 0·33 and 0·46, respectively. The calculated equilibrium volume fraction of allotriomorphic ferrite that can form at 800°C was found to be 0·20, based on application of the lever rule to the paraequilibrium phase diagram. The thickness of allotriomorphic ferrite that can grow, assuming paraequilibrium carbon diffusion controlled growth, at a given temperature can be calculated using the following equation[4]

$$q = \alpha_1 t^{0.5} \quad \ldots \quad (6)$$

where q is the half thickness of allotriomorphic ferrite, α_1 is the one dimensional parabolic thickness of ferrite, and t is the time (in seconds).

The calculation using the above equation indicates that, for a holding time of 10 min after the initiation of allotriomorphic growth, the thickness of ferrite should be about 6·42 μm. As can be seen from Table 5, the time required for a detectable amount of transformation is much higher relative to the time at T_1. Thus, some of the ferrite might have formed while cooling from 800°C to T_2. Therefore, it is not possible to control the allotriomorphic ferrite reaction because of the low hardenability used. However, this does not affect the concept of the experiment, providing that the amount of allotriomorphic ferrite that forms before bainite reaction is not excessive. The fact that the allotriomorphic ferrite forms during continuous cooling within the range T_1–T_2 is of no consequence, as shown by sample F6, which was cooled continuously from the austenite phase field by keeping the specimen within a sealed quartz tube and holding it in an ice–water mixture. This yielded a microstructure in which the austenite grain surfaces were decorated by thin layers of allotriomorphic ferrite and acicular ferrite (Figs. 7*a* and 7*b*). The similarity of the microstructure to that observed in the as deposited layers of ordinary C–Mn welds is considerable. The result emphasises the destruction of austenite grain boundary nucleation sites by allotriomorphic ferrite and shows its indirect effect in promoting the transformation of the remaining austenite to acicular ferrite.

EDX analysis (samples F6 and F5 in the TEM and the SEM, respectively) revealed no discernible change in the bulk substitutional alloying element concentration during allotriomorphic ferrite growth (*see* Table 7) within experimental error. The areas which were subjected to EDX analysis in the TEM and SEM are shown in Fig. 8. The figure also shows the variation of chromium, manganese, and silicon across the allotriomorphic ferrite. This indicates that the allotriomorphic ferrite has inherited the original substitutional alloying element concentration, consistent with a paraequilibrium growth mechanism. (Paraequilibrium is a constrained equilibrium where two phases, here α and γ, have the same substitutional atom/iron atom ratio, but which achieve equilibrium with respect to carbon. Thus, the growth of ferrite will be controlled by diffusion of carbon ahead of the α/γ interface.[26–28] The carbon extraction replicas have failed to show any presence of carbides in the transformed samples. This supports the assumption, made in deriving equation (1), that the transformation to bainite is associated with no precipitation of carbides. The replicas were found to contain only inclusions (since the samples were taken originally from weld metal portion) of complex manganese silicon oxides. Table 7 also gives a summary of EDX analysis on inclusions in sample F5.

DILATOMETRY

The variety of microstructures obtained with changing austenite grain size is shown in Figs. 9 and 10. As expected, those specimens austenitised at the higher temperature of 1150°C for 10 min transformed into allotriomorphic ferrite and acicular ferrite, whereas the others, austenitised at 1000°C for 10 min, transformed predominantly into a classical bainitic microstructure with a very small amount of allotriomorphic ferrite. The important observation again is that the presence of substantial amounts of acicular ferrite was associated with that of austenite grain boundary allotriomorphic ferrite.

The isothermal transformation experiments detailed in Table 6 were analysed further by plotting the relative length changes recorded during transformation as a function of the transformation temperature. To allow for any reaction before reaching T_i, data at T_i were converted by linearly extrapolating the $(\Delta L/L)$–T curve for the temperature range

Table 7 Results of microanalysis on allotriomorphic-acicular ferrite regions and inclusions in some furnace experiments

Alloying element	Sample	Observed concentration (mean), wt-%	Standard deviation	Matrix concentration, wt-%	Analysed region	Method
Manganese	F5	1·15	0·09	1·11	Allotriomorphic-acicular ferrite colony	SEM
Chromium	F5	1·71	0·07	1·59		
Silicon	F5	0·44	0·51	0·51		
Manganese	F6	1·24	0·13	1·11	Allotriomorphic-acicular ferrite colony	TEM
Chromium	F6	1·74	0·14	1·59		
Silicon	F6	0·54	0·08	0·51		
Manganese	F5	65·1	8·8	1·11	Inclusions (carbon replica)	TEM
Chromium	F5	0·98	0·71	1·59		
Silicon	F5	26·76	9·1	0·51		
Titanium	F5	5·4	5·0	0·009		

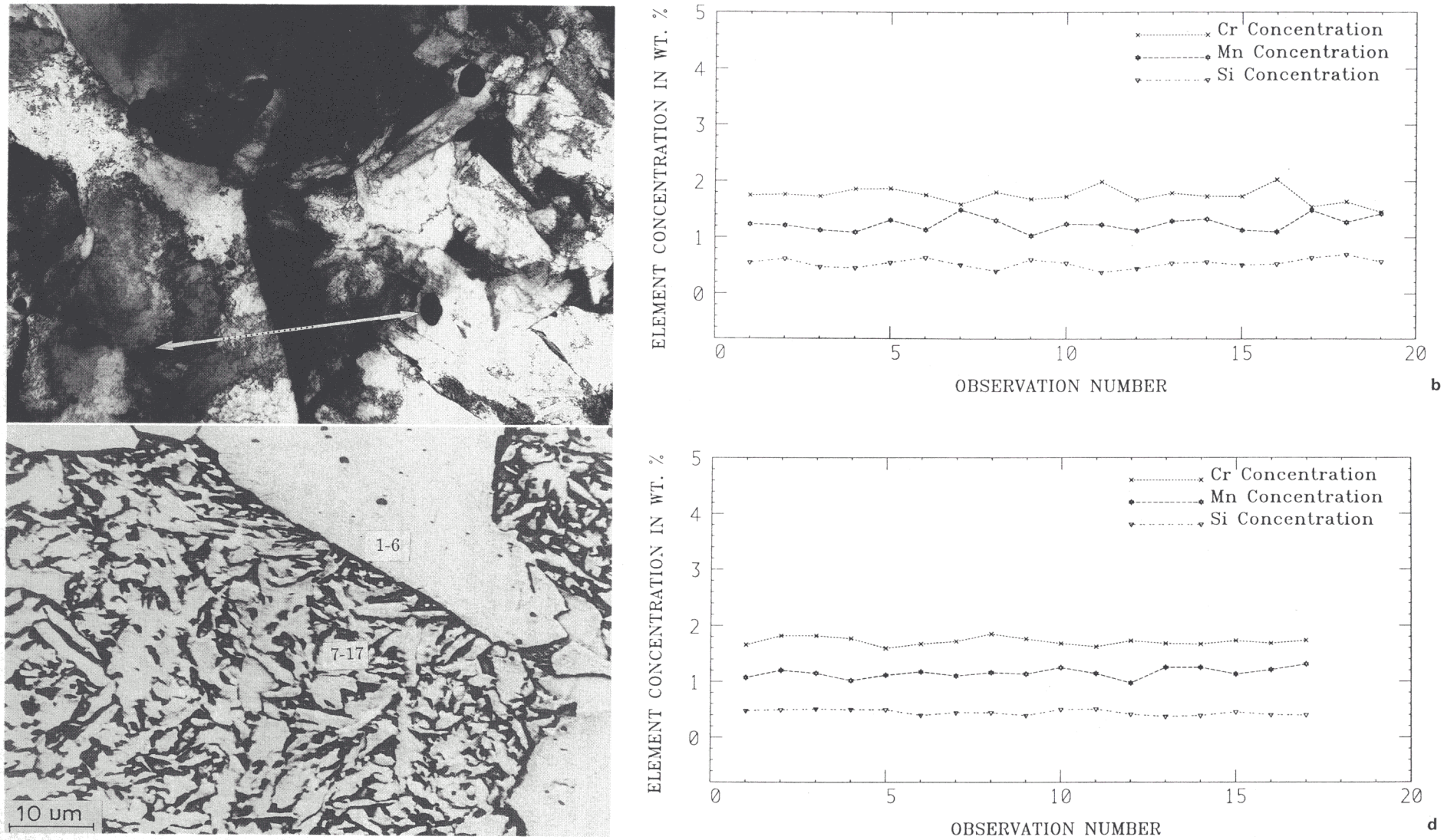

a region analysed by EDX in TEM (in sample F6) across allotriomorphic ferrite and acicular ferrite colony – line represents region over which analysis was carried out; *b* variation of Si, Mn, and Cr as measured by EDX analysis over line shown in *a*: first 10 points correspond to allotriomorphic ferrite region and others to acicular ferrite colony: variation shows no systematic change in alloying element concentration; *c* allotriomorphic ferrite and acicular ferrite microstructure as observed in SEM, which was subjected to EDX analysis; *d* variation of Si, Mn, and Cr as measured by EDX analysis over spots shown in *c*: points 1–6 correspond to analysis obtained from allotriomorphic ferrite region and others are from acicular ferrite region

8 Details of EDX analysis on samples from furnace experiments

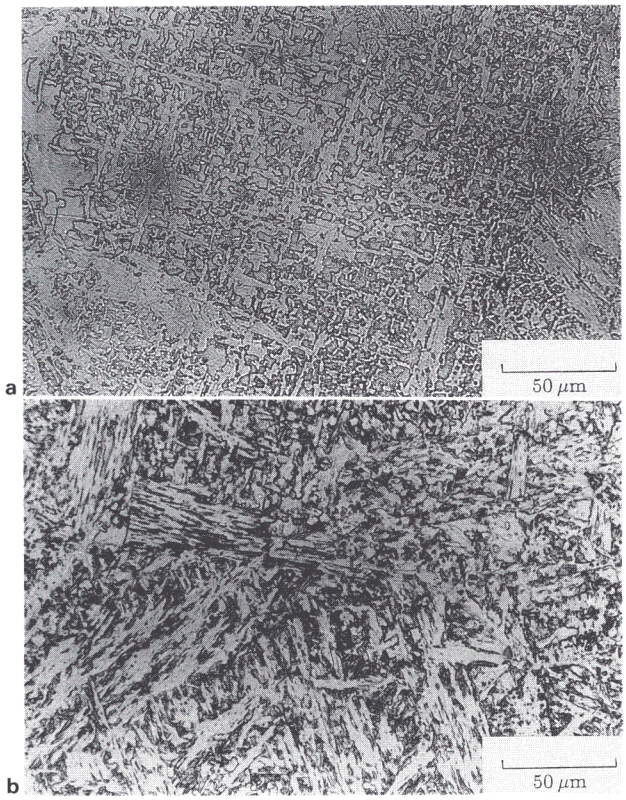

a L1 showing effect of allotriomorphic ferrite on promoting acicular ferrite; *b* S1 microstructure is predominantly bainite – no grain boundary allotriomorphic ferrite can be seen

9 Comparison of microstructure of isothermally transformed samples from dilatometric experiments

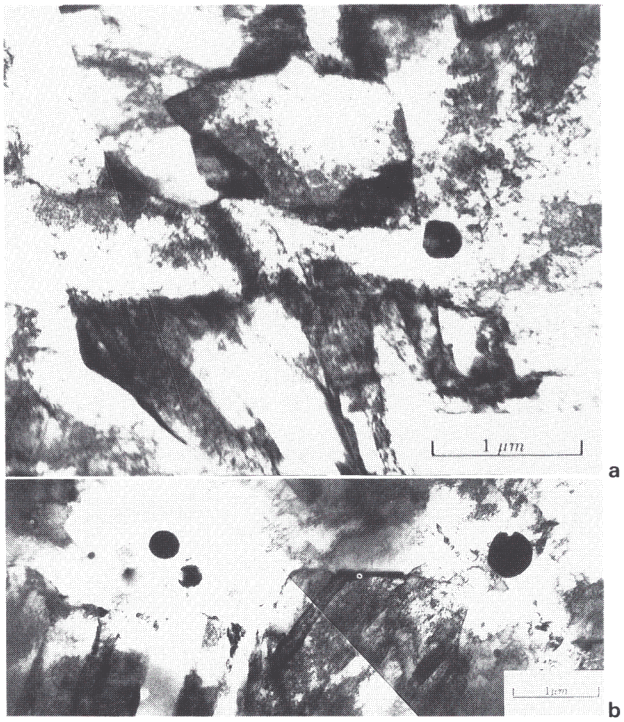

a L1 showing typical acicular ferrite plates nucleating from inclusion and also impingement of one plate with nearby plates; *b* S1 showing bainitic sheaf structure nucleating from prior γ/γ interface – inclusions can also be seen along grain boundary

10 Samples transformed isothermally in dilatometric experiments (TEM)

$T_\gamma - T_i$. This is shown schematically in Fig. 11; the actual curves are shown in Fig. 12. The length changes recorded at T_i and those estimated by extrapolation to T_i were analysed further to deduce the degree of reaction at T_i (*see* Table 8). The calculations also enable the carbon concentration in the residual austenite to be estimated, i.e. the experimental x_γ, which are marked on the calculated phase diagram shown in Fig. 13. The relative length change data obtained for all the dilatometric experiments indicate that some transformation could not be avoided before reaching T_i. As pointed out above, this is not important providing the total volume fraction of allotriomorphic ferrite is not very large.

Discussion

It appears that, for the austenite grain size range studied here, the alloy used transforms into bainite (samples F3, S1, and S2) provided that the austenite grain boundaries are free to nucleate bainite. However, the transition from bainite to acicular ferrite can be stimulated by eliminating the austenite grain boundary nucleation sites (samples F4, F5, L1, and L2). The γ/γ boundaries were destroyed in effect by the formation of thin layers of grain boundary allotriomorphic ferrite in both adjacent γ grains. The transformation mechanisms for both acicular ferrite and bainite are also found to be similar, as confirmed by dilatometric experiments which gave results similar to those of Yang and Bhadeshia.[9] The reaction clearly stopped at the point where $x_\gamma = x_{T_0'}$.

The important new observation is connected with the effect of the prior phase transformation to allotriomorphic ferrite. For the present alloy, the overall hardenability is low compared with the alloys studied by Yang and Bhadeshia.[9] Since allotriomorphic ferrite was not observed in their experiments, the observed transition from bainite

Table 8 Volume fraction calculations

Experiment	$\left(\frac{\Delta L}{L}\right)_{max}$	Volume fraction transformed V	(Experimental) mole fraction x_γ	T_i, °C
S1	0·0045	0·58	0·0053	505
S2	0·0042	0·54	0·0049	519
L1	0·0039	0·50	0·0045	513
L2	0·0035	0·45	0·0041	529

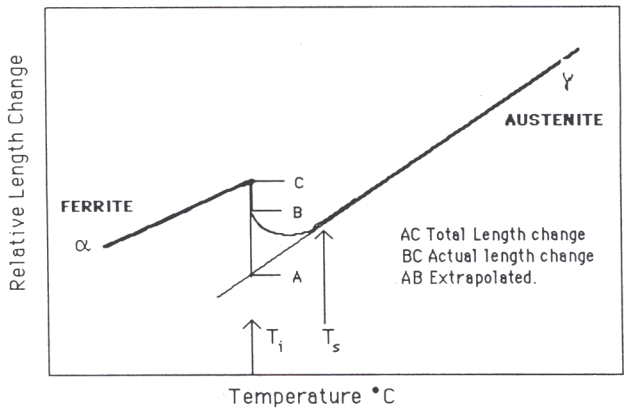

11 Schematic diagram of extrapolation method to calculate maximum relative length change at T_i, given case where there is transformation before reaching T_i while cooling from austenite phase field; dark line indicates actual relative length change

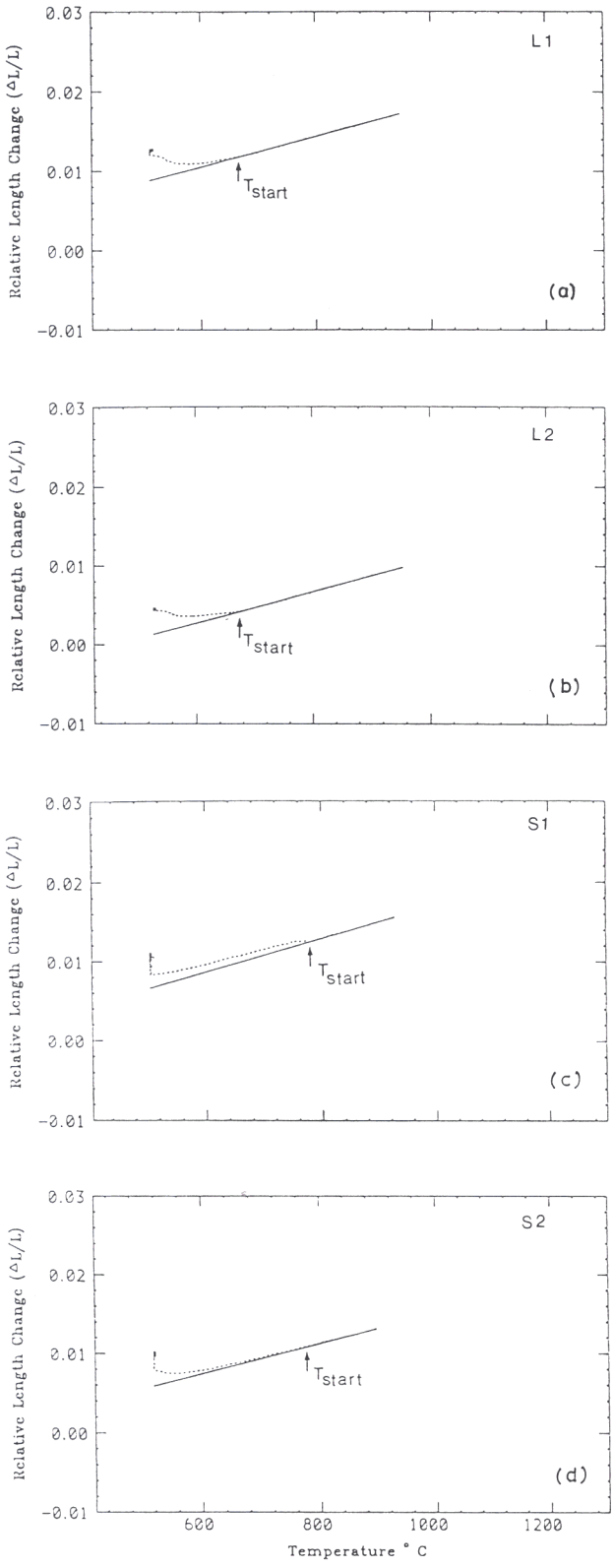

a, b after T_s, transformation rate seems to be very high, as shown by its rate of slope change of actual $(\Delta L/L)-T$ curve from extrapolated straight line, indicating allotriomorphic ferrite transformation while cooling from T_γ; this is also supported by high Δt_{850-T_i} (*see* Table 6); *c, d* although transformation started at very high temperature, as seen from graphs, because of less Δt_{850-T_i} (Table 6), transformation to allotriomorphic ferrite was comparatively low; this can be deduced from rate of slope change of actual $(\Delta L/L)-T$ curve with respect to extrapolated straight line

12 Comparison of $(\Delta L/L)-T$ plots for dilatometric experiments *a* L1, *b* L2, *c* S1, *d* S2 detailed in Table 6; plots show transformation start temperature and extrapolation procedure for calculating maximum length change at T_i

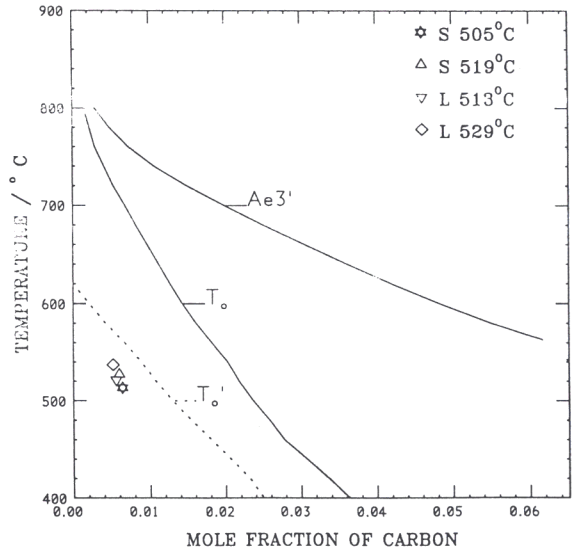

S, L low T_γ, high T_γ specimens, respectively

13 Comparison of experimental x_γ points corresponding to maximum volume fraction of ferrite for dilatometric experiments and phase boundary line calculated by Bhadeshia[12,13]

to acicular ferrite with increasing grain size could be attributed simply to the decrease in grain boundary sites for the nucleation of bainite; as is well established, classical bainite nucleation starts at the γ/γ grain boundaries.[29]

Thus, the present work gives an explanation of why high chromium welds tend to contain mostly bainite. Since the increase in chromium concentration reduces and eventually eliminates allotriomorphic ferrite, the austenite grain boundaries are free to nucleate the bainite before acicular ferrite can form intragranularly on the inclusions (Fig. 14).

Since both acicular ferrite and bainitic ferrite reactions were found to terminate when x_γ reached $x_{T_0'}$, the results confirm that the transformation mechanisms for bainitic ferrite and acicular ferrite are similar. Thin film carbon replica analysis failed to show any carbide precipitation in all samples, supporting the assumption inherent in equation (1). The experimentally measured carbon concentrations in the residual austenite at the point where the growth of acicular ferrite stopped were found to be somewhat lower than those estimated from the computed T_0' phase boundary (Fig. 13). This may be a consequence of a higher value of stored energy than that of 400 J mol^{-1} used in the present calculations.

The present results emphasise the fact that reactions taking place in the γ/γ grain boundaries can be crucial in determining the microstructures that develop in the weld metal. The ratio of the grain boundary and intragranular nucleation site densities can be modified to obtain the desired microstructure on transformation from austenite. The ability of inclusions to induce intragranular acicular ferrite is now a well established concept, although the nature and mechanism are not clear.[1,30–34] Removal of inclusions clearly causes an acicular ferrite microstructure to change to one which contains bainite.[11] This is also apparent in the measured continuous cooling transformation (CCT) diagrams published by Homma *et al.*,[35] which indicate that, in the absence of oxide inclusions, austenite transforms into bainitic ferrite or Widmanstätten ferrite (Fig. 15). These two mechanisms are shown schematically in Fig. 14.

A search of the literature revealed that chromium and molybdenum are not the only elements to induce the formation of bainite at the expense of acicular ferrite.

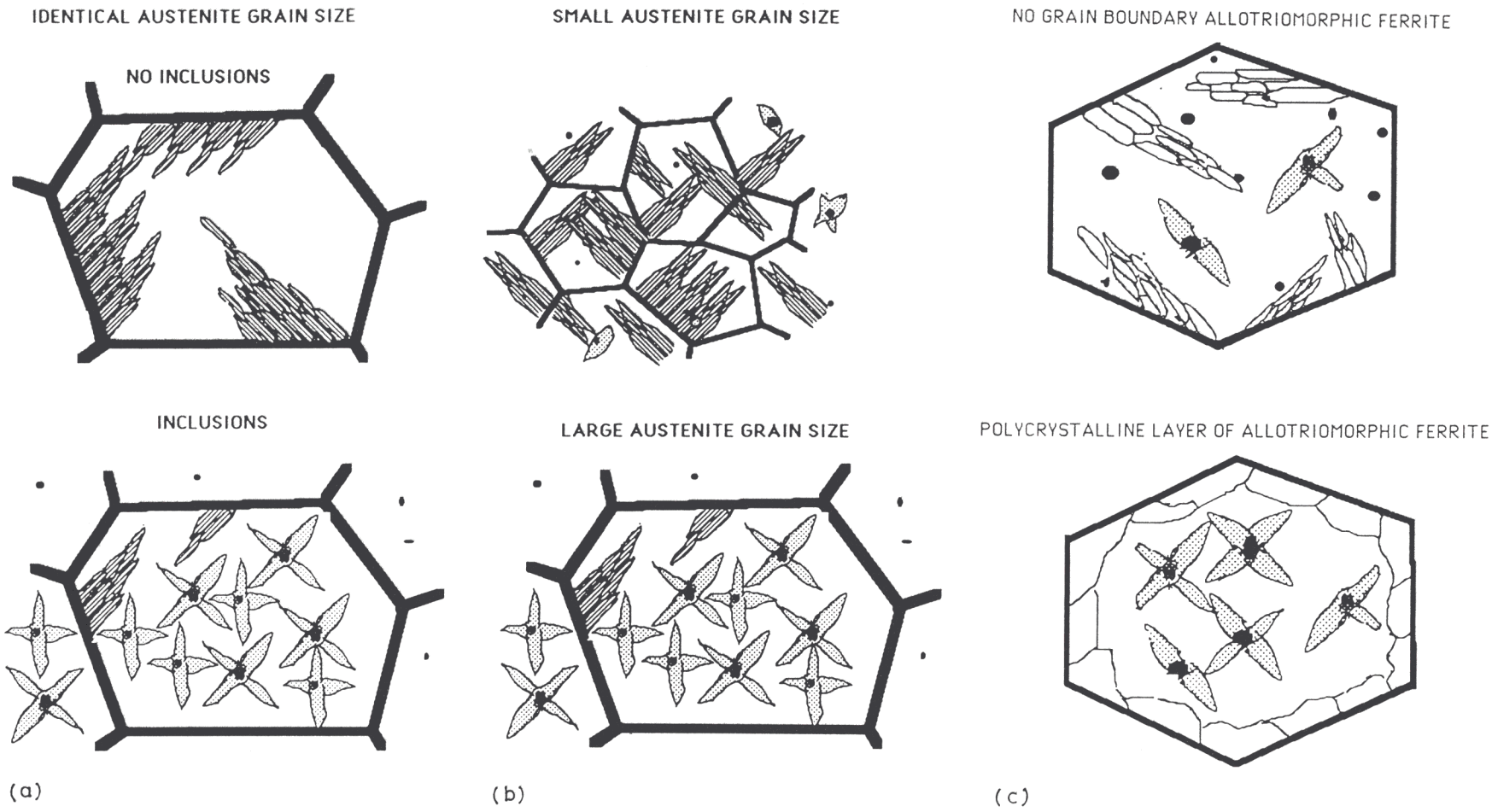

a effect of varying inclusion density for same austenite grain size; *b* effect of varying austenite grain boundary nucleation site density (grain size effect); *c* effect of prior transformation to allotriomorphic ferrite for same austenite grain size

14 Schematic diagram of mechanisms of transition from acicular ferrite to bainite (previously published and present results)

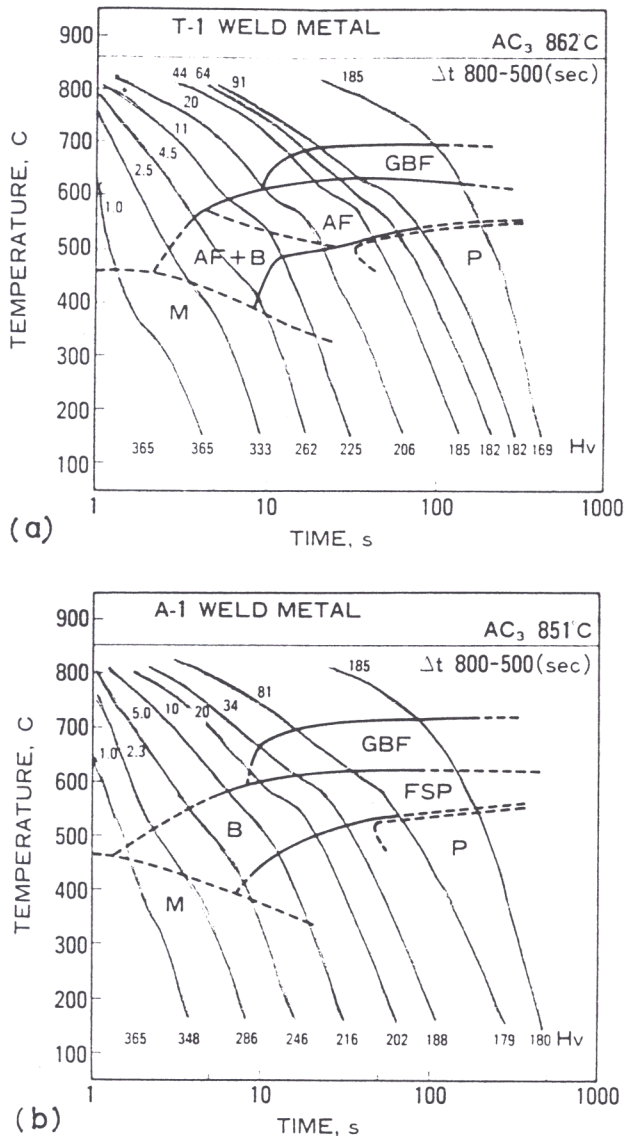

B bainite; AF acicular ferrite

15 Comparison of CCT diagrams for weld metal *a* containing Ti_2O_3 and *b* Ti_2O_3 free: presence of Ti_2O_3 promotes formation of acicular ferrite (After Ref. 35)

Similar effects can be deduced for manganese at high concentrations from the work by Horii *et al.*[36] and Grong *et al.*[37] In the latter work, the ferrite with aligned second phase (i.e. Widmanstätten ferrite or bainite) content was found to decrease with increase in manganese, as the acicular ferrite content increased. However, after an optimum level of manganese, the acicular ferrite began to be replaced to an increasing extent by ferrite with aligned second phase, as the volume fraction of grain boundary allotriomorphic ferrite also decreased.

It remains to be explained why the layers of allotriomorphic ferrite themselves appear incapable of nucleating bainite. The reason could be associated with the fact that the α/γ interface may not be stationary at the temperature T_2. However, this is an unlikely explanation, since the reconstructive transformation of austenite to allotriomorphic ferrite is extremely sluggish at the temperatures at which bainite forms. The alternative explanation is that the solute field, owing to elements displaced by the α into the adjacent γ, prevents the nucleation of bainite. If the growth of allotriomorphic ferrite is considered to occur by a paraequilibrium mechanism, then only the carbon composition profile ahead of the interface must be considered. With this assumption, consistent with the microanalysis data, allotriomorphic ferrite growth can be considered to be controlled by diffusion of carbon in the austenite ahead of the interface. The carbon composition profile in front of the moving interface can be calculated for various temperatures using the following equation[38]

$$x\{X,t\} = \bar{x} + (x^{\gamma\alpha} - \bar{x})E_1\{X,\underline{D}\} \quad \ldots\ldots (7)$$

where

$$E_1\{X,\underline{D}\} = \left[\frac{1-\mathrm{erf}\{X/(4\underline{D}t)^{0\cdot5}\}}{1-\mathrm{erf}\{Z/(4\underline{D}t)^{0\cdot5}\}}\right] \quad \ldots\ldots (8)$$

where X is the distance ahead of the moving α/γ interface, Z is the thickness of the allotriomorphic ferrite grown after a time t from the initiation of growth, and $\underline{D}$ is the weighted average diffusivity of carbon in austenite given by Trivedi and Pound[15]

$$\underline{D} = \int_{x^{\gamma\alpha}}^{\bar{x}} \frac{D\{X\}}{(\bar{x} - x^{\gamma\alpha})} \quad \ldots\ldots (9)$$

where $x^{\gamma\alpha}$ is the phase boundary composition given by the tie line of the calculated phase diagram (*see* Fig. 2). The term $D\{X\}$ is calculated based on the method of Siller and McLellan[39,40] and Bhadeshia.[41] The method takes into account the concentration dependence of the activity of carbon in austenite and the existence of finite repulsive interaction between nearest neighbouring carbon atoms situated in octahedral sites. The thickness of the allotriomorphic ferrite can be predicted using equation (6). Since the growth took place while cooling, the values of Z and other variables should correspond to a condition where the allotriomorphic ferrite growth ceases. To simplify the problem, the theoretical analysis was carried out for two cases: (i) the static case in which, on cooling from T_1 to T_2, the carbon composition profile in the austenite does not change at T_2 and (ii) the dynamic case when the carbon tries to diffuse from a carbon enriched sessile α/γ interface to a more homogeneous composition throughout the residual austenite.

STATIC CASE

It is possible that the region of carbon enriched austenite in the vicinity of the allotriomorphic ferrite/austenite interface suppresses the nucleation of bainite at that interface. As the allotriomorphic ferrite formation temperature decreases, $x^{\gamma\alpha}$ increases and the W_s, B_s, and M_s temperatures of austenite of composition $x^{\gamma\alpha}$ decrease, as shown in Fig. 16*b*. The transformation temperatures were all calculated according to Bhadeshia.[12,13] If the isothermal transformation temperature T_2 is above the calculated W_s or B_s temperatures for the austenite at the α/γ interface, then it can be concluded that the interface is incapable of nucleating Widmanstätten ferrite or bainite. Such a situation arises for all temperatures below the point marked A ($\sim 720°C$) on Fig. 16*b*. Since, in the present study, T_2 was always below 720°C, the calculations are consistent with the result that no Widmanstätten ferrite or bainite could be observed to nucleate from α/γ interfaces, thus making the allotriomorphic ferrite ideal for the purpose of stimulating the intragranular growth of α_a.

DYNAMIC CASE

The above model may not be valid if the carbon concentration profile at the α/γ interface homogenises during heat treatment at T_2. The growth of allotriomorphic ferrite becomes very sluggish indeed at temperatures below B_s and it is assumed here that it actually stops, thereby providing opportunity for homogenisation. A finite difference method (*see* Appendix) was used to test whether the

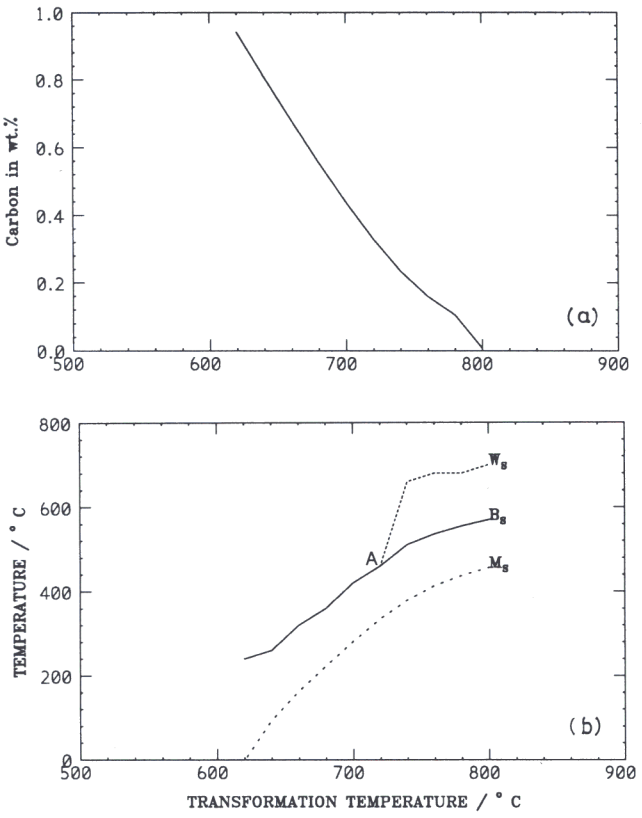

a variation in $x^{\gamma\alpha}$ as function of temperature at which allotriomorphic ferrite grows; *b* variation in W_s, B_s, and M_s temperatures of austenite at allotriomorphic ferrite/austenite interface as function of transformation temperature at which allotriomorphic ferrite grows by paraequilibrium transformation

16 Condition for nucleation of bainite at allotriomorphic ferrite/austenite interface; graph in *a* is essentially representation of Ae'_3 phase boundary line for present alloy; if T_2 is higher than calculated W_s or B_s, then nucleation of Widmanstätten ferrite or bainite is impossible (point A represents lowest allotriomorphic ferrite transformation temperature below which α/γ interface is found not to be capable of nucleating Widmanstätten ferrite or bainite)

carbon concentration profile, which develops during the growth of allotriomorphic ferrite at T_1, changes sufficiently on holding at T_2 to allow the austenite in the vicinity of the α/γ interface to decompose to bainite. The initial composition profile was established using equation (7) and by assuming that the allotriomorphic ferrite thickness is about 5 μm.

The calculations are carried out for $T_1 = T_C$, where T_C is the temperature at which the upper and lower C curves of the TTT diagram intersect. At T_C, displacive reactions become kinetically favourable after reconstructive transformations, so that T_C can be assumed to be the temperature at which the allotriomorphic ferrite growth stops. The homogenisation of carbon on subsequent treatment at $T_2 = 470°C$ is shown in Figs. 17 and 18. Even after holding for 120 s at T_2 (the longest reaction time used in the experiments), the calculations proved that the carbon content in the enriched austenite at the α/γ interface remains sufficiently high to prevent the formation of bainite.

It is of interest to examine other possible methods for rendering the austenite grain surfaces ineffective as possible bainite nucleation sites. The work of Mori *et al.*,[42] Snieder and Kerr,[43] and Fleck *et al.*,[44] in which boron is used as an alloy addition, is relevant in this respect. Finally, it should be noted that it may not be necessary to cover completely the austenite grain boundaries with allotriomorphic ferrite, since the ferrite will nucleate first at the most potent sites, thus eliminating them for the purpose of bainite nucleation. It is also relevant to point out that less than half of the allotriomorphic ferrite is likely to be in a crystallographic orientation suitable for stimulating α_W or α_b growth, even if the enriched austenite of γ at the α/γ interface did not prevent such growth. The reported increase in the acicular ferrite by Snieder and Kerr,[43] using boron additions, implies that the procedure could be considered for stimulating acicular ferrite in Fe–Cr–Mo–C welds also.

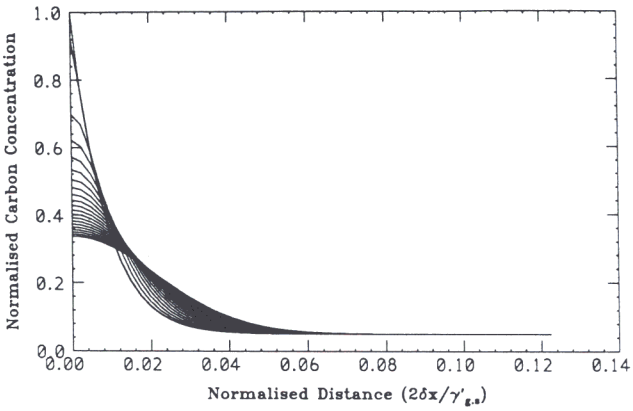

17 Cascade of whole carbon composition profile ahead of α/γ interface for time period of 120 s at $T_2 = 470°C$, showing that carbon composition neither becomes homogenised nor reduces to such a level that point A could be reached as in static case (this analysis assumes there is no change in interface composition as it cools to T_2): graph was drawn by normalising, changing interface composition with respect to initial interface composition and distance by half value of γ'_{gs} (residual austenite grain size); initial composition profile was calculated (*see* text) for allotriomorphic transformation temperature of 600°C

Conclusions

It is found that in weld metals containing inclusions the transition from bainite to acicular ferrite can be stimulated

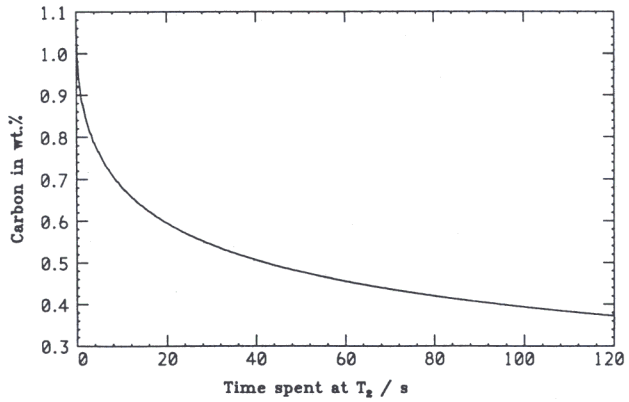

18 Cascade of interface composition only with respect to time at $T_2 = 470°C$: interface composition only drops to 0·358 wt-%, which is still less than point A (in Fig. 16*b*) for condition for nucleation of bainite at allotriomorphic ferrite/austenite interface (before this could be achieved, intragranular inclusions could stimulate formulation of acicular ferrite)

by the prior formation of a small amount of allotriomorphic ferrite along the austenite grain surfaces. This could be one of the main reasons why Fe–Cr–Mo–C welds tend to have predominantly bainitic microstructures at high alloy concentrations, since the allotriomorphic ferrite formation is then suppressed. Providing that the austenite grain boundaries are free to nucleate bainitic ferrite, the latter phase, in general, cannot be avoided and its formation will lead to a corresponding reduction in the quantity of acicular ferrite. It is probable that any allotriomorphic ferrite which is in an orientation relationship suitable for stimulating bainite, in fact, cannot do so, because the solute concentration in the enriched austenite at the allotriomorphic ferrite/austenite interface prevents it from transforming to bainite. This hypothesis has been confirmed using finite difference analysis, which indicated that the time taken for the carbon to homogenise is much higher than that required for α_a formation.

Acknowledgments

The authors wish to thank Professor D. Hull for providing the laboratory facilities at the University of Cambridge. Thanks are also due to Dr L.-E. Svensson, ESAB AB for providing the welds. One of the authors (SSB) also wishes to thank the Cambridge Commonwealth Trust for providing financial aid for this study and also the Council of Vice Chancellors and Principals of the United Kingdom for an overseas research students award.

References

1. H. K. D. H. BHADESHIA: in Proc. 2nd Int. Conf. 'Trends in welding research', Gatlingburg, TN, May, 1989, Keynote.
2. G. M. EVANS: IIW Doc. II-A-666-86, 1986.
3. G. M. EVANS: IIW Doc. II-A-739-88, 1988.
4. H. K. D. H. BHADESHIA, L.-E. SVENSSON, and B. GRETOFT: in Proc. 4th Scandinavian Symp. on 'Materials science', Trondheim, Norway, 25–26 Aug. 1986, Norwegian Institute of Technology, 153–158.
5. C. D. LUNDIN, S. C. KELLY, R. MENON, and B. J. KRUSE: *Weld. Res. Counc. Bull.*, 1986, **315**, 5.
6. J. T. MCGRATH, R. S. CHANDEL, R. F. ORR, and J. A. GIANETTO: *Can. Metall. Q.*, 1989, **28**, 75–83.
7. B. JOSEFSSON, A. KVIST, and H. O. ANDRÉN: *J. Phys.*, 1987, **C6**, 435.
8. H. K. D. H. BHADESHIA, L.-E. SVENSSON, and B. GRETOFT: *Acta Metall.*, 1985, **33**, 1271–1283.
9. J. R. YANG and H. K. D. H. BHADESHIA: in Proc. Conf. 'Advances in welding science and technology', 209–213; 1987, Metals Park, OH, ASM.
10. M. STRANGWOOD and H. K. D. H. BHADESHIA: in Proc. Conf. 'Advances in welding science and technology', 187–191; 1987, Metals Park, OH, ASM.
11. P. L. HARRISON and R. A. FARRAR: *J. Mater. Sci.*, 1981, **16**, 2218–2226.
12. H. K. D. H. BHADESHIA: *Acta Metall.*, 1981, **29**, 1117–1130.
13. H. K. D. H. BHADESHIA: *Met. Sci.*, 1982, **16**, 159–165.
14. A. A. B. SUGDEN and H. K. D. H. BHADESHIA: *Mater. Sci. Technol.*, 1989, **5**, (10), 977–984.
15. R. TRIVEDI and G. M. POUND: *J. Appl. Phys.*, 1967, **38**, 3569–3576.
16. M. STRANGWOOD and H. K. D. H. BHADESHIA: in Proc. Conf. 'Welding metallurgy of structural steels', 495–504; 1987, Warrendale, PA, The Metallurgical Society of AIME.
17. H. K. D. H. BHADESHIA: *J. Phys.*, 1982, **43-C4**, 435.
18. R. B. MCLELLAN and W. W. DUNN: *J. Phys. Chem. Solids*, 1969, **30**, 2631.
19. H. K. D. H. BHADESHIA: *Met. Sci.*, 1982, **16**, 167–169.
20. B. D. CULLITY: 'Elements of X-ray diffraction', 356; 1978, Reading, NY, Addison Wesley.
21. W. C. LESLIE: 'The physical metallurgy of steels', Int. Stud. edn, 111; 1982, New York, McGraw-Hill.
22. F. WEVER: *Z. Metallkd.*, 1928, **20**, 363–370.
23. H. K. D. H. BHADESHIA, S. A. DAVID, and J. VITEK: unpublished work, 1989.
24. H. K. D. H. BHADESHIA, and D. V. EDMONDS: *Metall. Trans.*, 1979, **10A**, 895–907.
25. H. K. D. H. BHADESHIA and D. V. EDMONDS: *Acta Metall.*, 1980, **28**, 1265–1273.
26. M. HILLERT: *Jernkontorets Ann.*, 1951, **135**, 403.
27. E. RUDBERG: *Jernkontorets Ann.*, 1952, **136**, 91.
28. H. I. A. AARONSON, H. A. DOMAIN, and G. M. POUND: *Trans. AIME*, 1966, **236**, 768.
29. H. K. D. H. BHADESHIA: in Proc. Conf. 'Phase transformations '87', 309–314; 1988, London, The Institute of Metals.
30. D. J. ABSON, R. E. DOLBY, and P. H. M. HART: in Proc. Conf. on 'Trends in steels and consumables for welding', London, Nov. 1979, The Welding Institute, 75–101.
31. J. M. DOWLING, J. M. CORBETT, and H. W. KERR: *Metall. Trans.*, 1986, **17A**, 1611–1623.
32. R. A. RICKS, G. S. BARRITE, and P. R. HOWELL: in Proc. Conf. on 'Solid state phase transformation', 463–465; 1981, Pittsburgh, PA, AIME.
33. R. A. RICKS and G. S. BARRITE: *J. Mater. Sci.*, 1982, **17**, 732–740.
34. S. LIU and D. L. OLSON: *Weld. J.*, 1986, **65**, 139s–149s.
35. H. HOMMA, S. OHKITA, S. MATSUDA, and K. YAMAMOTO: *Weld. J.*, 1987, **66**, 301s–309s.
36. Y. HORII, S. OHKITA, M. WAKABAYASHI, and M. NAMURA: *Nippon Steel Tech. Rep.*, April 1988, no. 37, 3.
37. Ø. GRONG, T. A. SIEWART, and G. R. EDWARDS: *Weld. J.*, 1986, **65**, 282s.
38. D. E. COATES: *Metall. Trans.*, 1973, **4**, 395.
39. R. H. SILLER and R. B. MCLELLAN: *Trans. AIME*, 1969, **245**, 697–700.
40. R. H. SILLER and R. B. MCLELLAN: *Metall. Trans.*, 1970, **1**, 985–988.
41. H. K. D. H. BHADESHIA: *Met. Sci.*, 1981, **15**, 477–479.
42. N. MORI, H. HOMMA, S. OHKITA, and K. ASANO: IIW Doc. IX-1158-80, 1980.
43. G. SNIEDER and H. W. KERR: *Can. Metall. Q.*, 1984, **23**, 315–325.
44. N. A. FLECK, Ø. GRONG, G. R. EDWARDS, and D. K. MATLOCK: *Weld. J.*, 1986, **64**, 113s–121s.

Appendix

Finite difference method

The carbon composition profile build-up ahead of the allotriomorphic ferrite/austenite interface in the residual austenite is examined here using a finite difference method to simulate any homogenisation of concentration. The main advantage of the application of a finite difference method to this problem is that it can handle the changing boundary conditions during the homogenisation process. The finite difference method is based on the technique discussed by Crank.[45] The model assumes a one dimensional diffusion process ahead of a planar allotriomorphic ferrite/austenite interface. The initial profile setup at a time $t = 0$ is given by the analytical equation, as discussed in the main text. The composition profile is then subjected to a finite difference method after normalising the variables to dimensionless quantities suitable for this method. The normalised variables are as follows

$$\text{distance } X = \frac{x}{\left(\frac{\gamma_{gs}}{2} - q\right)}$$

$$\text{concentration } C = \frac{C_{i,j}}{C^{\gamma\alpha}}$$

$$\text{time } T = \frac{Dt}{x^2}$$

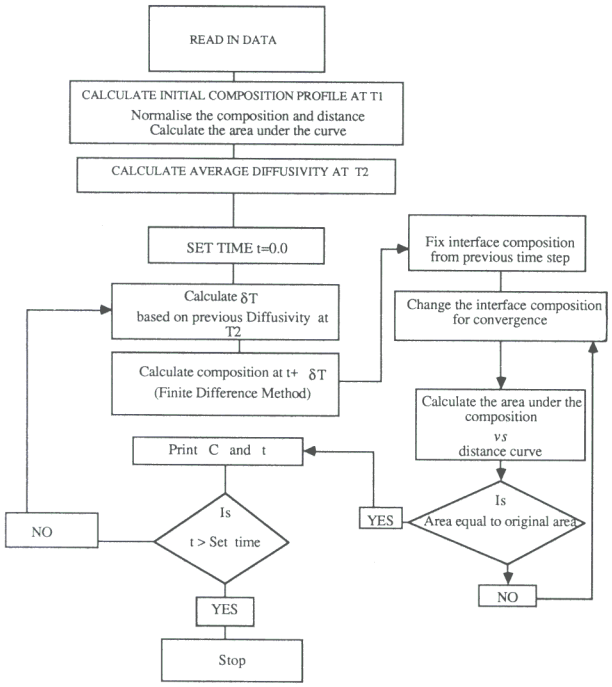

19 Flow chart indicating finite difference method for simulating cascade of interface composition with time

where x is the distance from the α/γ interface, q is the half thickness of ferrite, γ_{gs} is the austenite grain size, $C_{i,j}$ is the composition at any time step j and at position i from the interface, $C^{\gamma\alpha}$ is the composition of interface at $t = 0$, and $\underline{D}$ is the average diffusivity calculated for every time step δt. Here the interface position does not move with time, since allotriomorphic ferrite growth is assumed to be completed. The interface composition is determined for each time step by the mass balance. The area under the normalised composition profile is calculated using numerical integration. The general finite difference equation for the composition in the next time interval is

$$C^{\gamma}_{i,j+1} = C^{\gamma}_{i,j} + R(C^{\gamma}_{i-1,j} - 2C^{\gamma}_{i,j} + C^{\gamma}_{i+1,j})$$

where $R = \underline{D}\delta t/(\delta x)^2$ and is taken to be 0·1. This particular value was assumed after checking that the variation of coefficient R from 0·1–0·3 made little difference to the results. The term $C^{\gamma}_{i,j+1}$ is the composition at position i of interface and at a time step $j+1$ and is defined from the compositions at the $i-1, i, i+1$ positions at a time step j. The diffusivity for the next time step is calculated from the composition profile for the current time. The flow chart for the program is shown in Fig. 19.

Reference

45. J. CRANK: 'The mathematics of diffusion', 2 edn; 1975, Oxford, Clarendon Press.